Available online at www.sciencedirect.com
ScienceDirect
Journal of Sound and Vibration 312 (2008) 125–139
JOURNAL OF SOUND AND VIBRATION
www.elsevier.com/locate/jsvi

Analysis of in-plane wave propagation in hexagonal and re-entrant lattices

Stefano Gonella, Massimo Ruzzene*

School of Aerospace Engineering, Georgia Institute of Technology Atlanta, GA 30332-0150, USA

Received 14 April 2007; received in revised form 16 October 2007; accepted 19 October 2007
Available online 18 December 2007

Abstract

Plane wave propagation in hexagonal and re-entrant lattices is investigated through the application of Bloch's theorem. Two-dimensional dispersion relations are estimated and analyzed to illustrate peculiar properties of re-entrant configurations and investigate the directional behavior of hexagonal lattices for varying construction angles. Special attention is devoted to the determination of phase and group wave velocities. Velocity plots are obtained for varying frequency and direction of wave propagation to analyze the dispersion characteristics of the lattices and further investigate their directional characteristics.

1. Introduction

Lattice materials are cellular structures obtained from the assembly of beam elements, which can be either rigidly connected or joined through pins. Lattice materials of various topologies have been the object of extensive investigations, as they can be considered as simplified models for a number of structural systems found in various engineering fields. Examples of lattice-like materials and systems include, among others, honeycomb cores in sandwich panels, trusses, particulate filters, acoustic resonators, as well as simple idealizations for crystals or "latticed proteins". The investigation of the mechanical properties of lattice materials can take great advantage from their spatial periodicity. The analysis of the propagation of elastic waves in this class of structural assemblies can in fact be performed by applying techniques introduced in solid state physics [1]. Engineering applications of such techniques can be found in the extensive body of literature by Mead and coworkers, which is summarized in Ref. [2]. In periodic structures, the impedance mismatch generated by periodic discontinuities in geometry and/or material within the structure causes destructive wave interference phenomena over specified frequency bands called "stop-bands" or "bandgaps". Lattice materials are examples of two-dimensional (2-D) periodic structures. In 2-D periodic structures, the location and the extension of the bandgaps depend on the considered direction of wave propagation on the structure surface [3]. This unique directional behavior complements the bandgap characteristics of all periodic assemblies, and makes the application of 2-D periodic structures as directional mechanical filters extremely attractive. In this

*Corresponding author.
E-mail address: massimo.ruzzene@ae.gatech.edu (M. Ruzzene).

0022-460X/$ - see front matter © 2007 Elsevier Ltd. All rights reserved.
doi:10.1016/j.jsv.2007.10.033

regard, research has been conducted to relate specific unit cell configurations to particular behaviors in order to design lattices with given vibration isolation characteristics [4]. Other recent studies [5,6] have investigated the directional characteristics (“beaming”) of hexagonal lattices and of cylindrical grids. The propagation of in-plane elastic waves in various lattice structures is investigated in Ref. [8], and by Phani et al. [7], where a valuable comparison between equivalent mechanical properties available from the literature [9] and results from the wave propagation analysis is also presented. Noteworthy research has been conducted to study the effect of inclusions and the influence of nature and size of localized imperfections on the bandgap behavior of lattices [10]. The analysis of out-of-plane wave propagation in hexagonal lattices presented in Ref. [5] is here extended to evaluate the properties related to the propagation of in-plane waves. Particular emphasis is again placed on re-entrant honeycomb configurations, which are characterized by a negative in-plane Poisson’s ratio [11], and which in Ref. [5] have been found to feature superior directional characteristics. Special attention is also devoted to the determination of phase and group velocities. A combined inspection of velocity plots and phase constant surfaces is carried out to show the dependence of the directional behavior of lattices upon the geometry of the unit cell and the frequency of wave propagation.

The paper is organized as follows. In Section 1 a brief introduction is given. Section 2 provides a description of the geometry of different configurations of hexagonal lattices and presents the tools for the wave propagation analysis. Section 3 illustrates the wave propagation characteristics of hexagonal lattices, with emphasis on directionality and on wave velocities. Section 4 finally summarizes the main results of the work.

2. Unit cell analysis of wave propagation in 2-D lattices

We investigate the characteristics of wave propagation in hexagonal lattices of the kind shown in Fig. 1.

2.1. Description of lattice geometry and notational conventions

The lattices under investigation are obtained from the assembly of unit cells of the kind shown in Fig. 2. The geometry of the unit cell is defined by the internal angle θ, and by the ratios $\alpha = H/L$ and $\beta = t/L$ which, respectively, define the relative cell wall length, and the walls’ slenderness ratio. A regular hexagonal lattice is defined by $\theta = 30^\circ$ and $\alpha = 1$, while re-entrant lattices of the kind shown in Fig. 1b are characterized by negative values of θ. As in any periodic assembly, the location of a generic point can be described in terms of location within a reference unit cell and a set of lattice vectors which define the periodicity of the assembly.

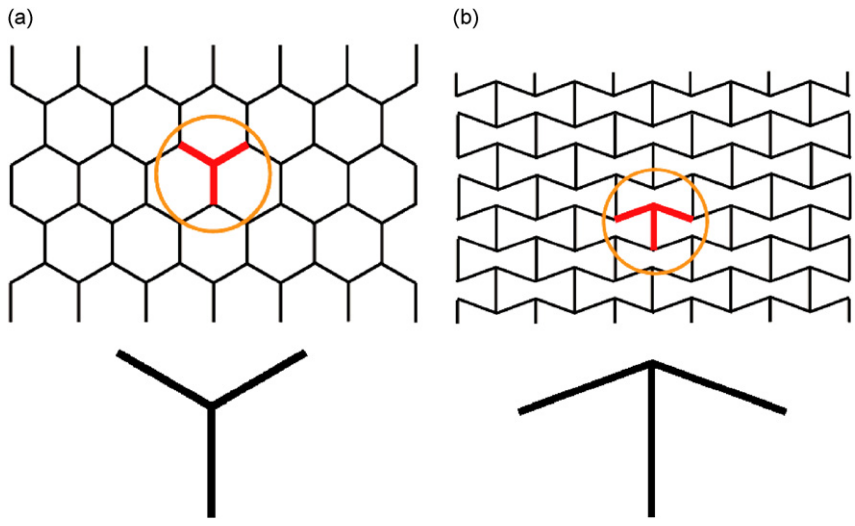

Fig. 1. Two types of lattices: (a) hexagonal and (b) re-entrant.

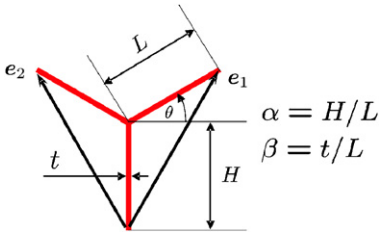

Fig. 2. Unit cell and its characteristics dimensions.

We introduce a reference frame in the plane of the lattice $\mathscr{F}_{\mathscr{I}}$ defined by a unit vector basis $\mathscr{I} = (\mathbf{i}_1, \mathbf{i}_2)$, such that the location of a point P in cell n_1, n_2 can be expressed as

$$\boldsymbol{\rho}_P(n_1, n_2) = \mathbf{r}_P + n_1\mathbf{e}_1 + n_2\mathbf{e}_2, \tag{1}$$

where $\mathbf{r}_P$ defines the position of the point corresponding to P in the reference cell $(0, 0)$, while $\mathbf{e}_1, \mathbf{e}_2$ are the lattice vectors. In here and in the following developments, vectors are denoted as bold, lower case letters, while matrices are denoted as bold capital letters. Also, the notation $()^A$ indicates components with respect to the vector basis A. Accordingly, the lattice vectors can be expressed as

$$\mathbf{e}_1^{\mathscr{I}} = (L\cos\theta, H + L\sin\theta)^{\mathrm{T}},$$

$$\mathbf{e}_2^{\mathscr{I}} = (-L\cos\theta, H + L\sin\theta)^{\mathrm{T}}. \tag{2}$$

2.2. Bloch's theorem

Wave propagation in systems of the kind depicted in Fig. 1 is traditionally studied through the application of Bloch's theorem. The displacement $\mathbf{w}$ of a point P of the reference unit cell corresponding to a wave propagating at frequency ω can be expressed as

$$\mathbf{w}(\mathbf{r}_P) = \mathbf{w}_{P_0} \mathrm{e}^{\mathrm{i}\omega t - \mathbf{k}\cdot\mathbf{r}_P}, \tag{3}$$

where $\mathbf{w}_{P_0}$ is the wave amplitude, and $\mathbf{k}$ is the wave vector. According to Bloch theorem, the displacement of the point corresponding to P at location $\boldsymbol{\rho}_p(n_1, n_2)$ can be written in terms of the displacement of the reference unit cell as follows:

$$\begin{aligned} \mathbf{w}(\boldsymbol{\rho}_P) &= \mathbf{w}(\mathbf{r}_P)\mathrm{e}^{\mathbf{k}\cdot(\boldsymbol{\rho}_P - \mathbf{r}_P)} \\ &= \mathbf{w}(\mathbf{r}_P)\mathrm{e}^{n_1k_1 + n_2k_2}, \end{aligned} \tag{4}$$

where $k_i = \mathbf{k}\cdot\mathbf{e}_i$ with $i = 1, 2$. Bloch's theorem states that the proportionate change in wave amplitude occurring from cell to cell does not depend on the cell location within the periodic system. Accordingly, the wave propagation characteristics of the periodic assembly can be fully identified through the analysis of the reference unit cell. In Eq. (4), $k_i = \delta_i + i\varepsilon_i$ $(i = 1, 2)$ is a complex number, whose real part δ_i defines the amplitude attenuation as a wave propagates from one cell to the next, while the imaginary part ε_i defines the change of phase across each cell and it is therefore often called *phase constant*. In the analysis of wave propagation without amplitude attenuation, δ_i is typically set to 0, while the phase constants ε_i are varied to investigate their dependency upon frequency.

The space defined by the lattice vector basis $\mathscr{E} = (\mathbf{e}_1, \mathbf{e}_2)$ is denoted as the *direct lattice*. Given a direct lattice space, one may define a reciprocal lattice, which is described by the basis $\mathscr{B} = (\mathbf{b}_1, \mathbf{b}_2)$, whose basis vectors are given by

$$\mathbf{b}_i \cdot \mathbf{e}_j = \delta_{ij}, \tag{5}$$

where δ_{ij} is the Kronecker delta. The reciprocal lattice vectors for the hexagonal lattices under consideration are given by

$$\mathbf{b}_1^{\mathscr{I}} = \left(\frac{1}{2L\cos\theta}, \frac{1}{2(H+L\sin\theta)}\right)^{\mathrm{T}},$$
$$\mathbf{b}_2^{\mathscr{I}} = \left(-\frac{1}{2L\cos\theta}, \frac{1}{2(H+L\sin\theta)}\right)^{\mathrm{T}}. \tag{6}$$

In the reciprocal lattice, the wave vector $\mathbf{k} = 2\pi\boldsymbol{\lambda}$ can be expressed as

$$\mathbf{k} = k_1\mathbf{b}_1 + k_2\mathbf{b}_2, \tag{7}$$

so that, according to the definition of reciprocal lattice given in Eq. (5):

$$\mathbf{k}\cdot\mathbf{e}_1 = k_1. \tag{8}$$

While the direct lattice defines the spatial periodicity of the considered domain, the reciprocal lattice describes the periodicity of the frequency/wavenumber relation. This can be easily demonstrated by replacing $\boldsymbol{\lambda}$, where $\mathbf{k} = 2\pi\boldsymbol{\lambda}$, with $\boldsymbol{\lambda}' = \boldsymbol{\lambda} + m_1\mathbf{b}_1 + m_2\mathbf{b}_2$ in Eq. (4), with m_1, m_2 integers. This gives:

$$\mathbf{w}(\boldsymbol{\rho}_p) = \mathbf{w}(\mathbf{r}_p)\mathrm{e}^{n_1k_1'+n_2k_2'},$$

where

$$k_i' = 2\pi\boldsymbol{\lambda}'\cdot\mathbf{e}_i = k_i + 2\pi m_i, \quad i = 1,2, \tag{9}$$

which shows that the wavenumber in a 2-D lattice is a periodic function of the wave vector $\mathbf{k}$ in the reciprocal lattice. Hence, full representation of the dependency of the wave vector upon the frequency of wave propagation is obtained by investigating its variation over a single period. In a 2-D lattice, the period corresponds to a region in the reciprocal lattice whose area equals the area of the reciprocal lattice's unit cell. The procedure for the identification of the area corresponding to the period, also known as *first Brillouin zone*, is described in Ref. [1]. Examples of first Brillouin zones for a regular hexagonal lattice and for re-entrant lattices are presented in the following section.

2.3. Analysis of free wave motion

2.3.1. Dispersion relations

The behavior of the unit cell of the periodic domain can be conveniently described through its discretized equation of motion and by defining the cell's interaction with its neighbors (Fig. 3). The unit cell is modeled as an assembly of rigidly connected beams, whose behavior is described by the set of degrees of freedom depicted

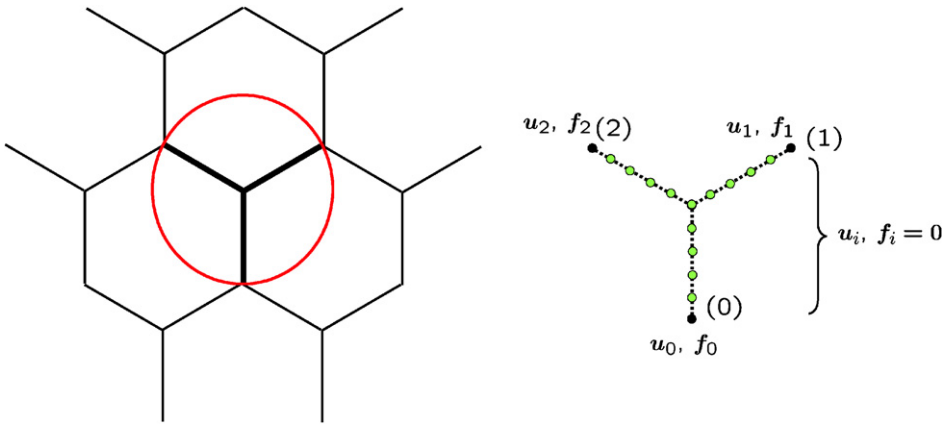

Fig. 3. Unit cell degrees of freedom and interaction with neighboring cells.

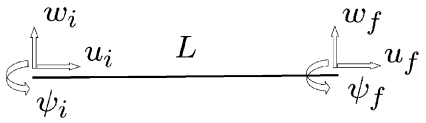

Fig. 4. Element degrees of freedom.

in Fig. 4. Application of standard Finite Element procedures yields the unit cell's equation of motion, which can be expressed as

$$(\mathbf{K} - \omega^2\mathbf{M})\mathbf{u} = \mathbf{f}, \tag{10}$$

where ω is the frequency of wave propagation, $\mathbf{K}$ and $\mathbf{M}$ are the assembled mass and stiffness matrices for the cell, while $\mathbf{u}$, $\mathbf{f}$ are, respectively, the vectors containing generalized nodal displacements and forces of interaction of the cell with its neighbors (see Fig. 3):

$$\begin{aligned} \mathbf{u} &= \{\,\mathbf{u}_0 \quad \mathbf{u}_1 \quad \mathbf{u}_2 \quad \mathbf{u}_i\,\}^{\mathrm{T}}, \\ \mathbf{f} &= \{\,\mathbf{f}_0 \quad \mathbf{f}_1 \quad \mathbf{f}_2 \quad 0\,\}^{\mathrm{T}}. \end{aligned} \tag{11}$$

In Eq. (11) the subscripts 0, 1, 2 follow the notation described in Fig. 3, while subscript i denotes the degrees of freedom of nodes that are internal to the cell. Eq. (11) is also based on the assumption that no external forces are applied and that only the interaction forces with neighboring cells appear in the cell's equation of motion. The absence of external forces on the internal nodes facilitates the condensation of the internal degrees of freedom, which yields a significant reduction in the size of the problem. According to Bloch's theorem, periodicity conditions relate the cell's generalized displacements, in addition to equilibrium conditions which can be applied to the generalized forces:

$$\begin{aligned} \mathbf{u}_1 &= \mathrm{e}^{k_1}\mathbf{u}_0, \\ \mathbf{u}_2 &= \mathrm{e}^{k_2}\mathbf{u}_0 \end{aligned} \tag{12}$$

and

$$\begin{aligned} \mathbf{f}_1 &= -\mathrm{e}^{k_1}\mathbf{f}_0, \\ \mathbf{f}_2 &= -\mathrm{e}^{k_2}\mathbf{f}_0. \end{aligned} \tag{13}$$

Eqs. (12) and (13) can be rewritten in matrix form as follows:

$$\mathbf{u} = \mathbf{A}\mathbf{u}_r \tag{14}$$

$$\mathbf{f} = \mathbf{B}\mathbf{f}_r, \tag{15}$$

where $\mathbf{u}_r = \{\,\mathbf{u}_0 \quad \mathbf{u}_i\,\}^{\mathrm{T}}$. Substituting Eq. (12) into Eq. (10), pre-multiplying the resulting equations for $\mathbf{A}^H$, with $()^H$ denoting a complex transpose conjugate, and assuming $\mathbf{f}_i = 0$ gives:

$$[\mathbf{K}_r(k_1,k_2) - \omega^2\mathbf{M}_r(k_1,k_2)]\,\mathbf{u}_r = \mathbf{0}, \tag{16}$$

where $\mathbf{K}_r(k_1,k_2)$, $\mathbf{M}_r(k_1,k_2)$ are reduced stiffness and mass matrices. Eq. (16) is an eigenvalue problem whose solution defines the dispersion characteristics of the lattice. The solution requires imposing two of the three unknowns k_1, k_2, ω, and solving for the third. Typically, wave motion without attenuation is investigated. For this reason, k_1, k_2 are generally imposed as imaginary numbers $k_1 = i\varepsilon_1$, $k_2 = i\varepsilon_2$ which vary within the first Brillouin zone. The solution of the eigenvalue problem yields the frequency of wave propagation corresponding to the assigned pair k_1, k_2. The complete solution obtained for varying k_1, k_2 is a surface $\omega = \omega(k_1, k_2)$ denoted as *phase constant surface* or *dispersion surface*. The number of surfaces obtained corresponds to the dimension of the eigenvalue problem in Eq. (16). Each surface describes the wavenumber/frequency relation for the corresponding mode of wave propagation in the considered medium. The computational cost of the evaluation of the dispersion diagrams can be significantly reduced by exploiting the symmetry of the first Brillouin zone, which is related to the symmetry of the unit cell. As a result, smaller regions of variation for the phase constants can be identified. Such regions are denoted as *irreducible Brillouin*

zones. In addition, information regarding propagation in specific directions can be obtained by letting the wave vector vary only along the contour of the irreducible zone. For most periodic structures featuring a certain degree of symmetry, limiting the variation of the wavenumber along the contour of the Brillouin zone is known to be sufficient to highlight the presence and determine the entity of frequency gaps between consecutive phase constant surfaces (bandgaps). Although, to the author's knowledge, a rigorous proof of this is still not available, this procedure is widely accepted in the related literature. Moreover, the width of the bandgaps has been verified by evaluating gaps between subsequent branches of the dispersion relations. In all the cases, no counter example has been found, so the band diagrams have been chosen as an effective way of presenting the mode structure of the lattices. Examples of irreducible zones and various possible representations of the dispersion diagrams will be presented in the next section.

2.3.2. Phase and group velocities

The dispersion surfaces are used to estimate the variation of the phase and group velocity in terms of frequency and direction of wave propagation. The phase velocity in a direction defined by the wave vector:

$$\mathbf{k} = k_1\mathbf{b}_1 + k_2\mathbf{b}_2, \tag{17}$$

$$\mathbf{k} = \xi_1\mathbf{i}_1 + \xi_2\mathbf{i}_2 \tag{18}$$

and at frequency ω is given by

$$\mathbf{c}_{ph} = \frac{\omega}{k}\mathbf{u}, \tag{19}$$

where $k = |\mathbf{k}|$ and $\mathbf{u}$ is a unit vector in the direction of the wave vector ($\mathbf{u} = \mathbf{k}/k$). The phase velocity is evaluated by selecting the wavenumbers corresponding to the dispersion surfaces at the desired frequency value. The angular range spanned by the corresponding set of wavenumbers is then computed to obtain the variation of the phase velocity in terms of the direction of wave propagation. For a non-dispersive, homogeneous medium, this operation yields a circle whose radius is independent of frequency. The same information is commonly presented in the form of slowness curves, which are plots of the inverse of the phase velocity [12]. In the examples of the paper, however, it was chosen to directly represent variations of velocity in terms of direction of wave propagation and frequency. Such variations may also be directly observed from the time domain simulation of wave propagation within the cellular domain.

Important indications regarding the wave characteristics of a lattice are also provided by the group velocity, which can be also estimated from the dispersion surfaces. The group velocity in the direct lattice space can be expressed as

$$\mathbf{c}_g^{\mathscr{E}} = \left(\frac{\partial\omega}{\partial k_1}, \frac{\partial\omega}{\partial k_2}\right)^{\mathrm{T}}, \tag{20}$$

which can be transformed into components in the physical space $\mathscr{I}$ through a straightforward manipulation of vectors, which gives:

$$\mathbf{c}_g^{\mathscr{I}} = \begin{pmatrix} \mathbf{e}_1\cdot\mathbf{i}_1, & \mathbf{e}_2\cdot\mathbf{i}_1 \\ \mathbf{e}_1\cdot\mathbf{i}_2, & \mathbf{e}_2\cdot\mathbf{i}_2 \end{pmatrix}\mathbf{c}_g^{\mathscr{E}},$$

$$\mathbf{c}_g^{\mathscr{I}} = \mathbf{E}\mathbf{c}_g^{\mathscr{E}}, \tag{21}$$

where matrix $\mathbf{E}$ contains the components of the direct lattice basis with respect to the physical reference system $\mathscr{I}$. The group velocity defines the direction of energy flow within the structure, and therefore identifies preferential or forbidden directions for wave propagation [5]. In addition, the dispersive nature of the medium can also be highlighted from a discrepancy between group and phase velocity. Such a discrepancy can occur both for increasing frequency and, more interestingly, along different directions. At a given frequency, the lattice may behave in a dispersive fashion in a range of directions, while being non-dispersive in others. The characteristics of hexagonal lattices in terms of dispersion surfaces, phase and group velocity will be discussed in the next section. The evaluation of group and phase velocities allows determining the dispersive behavior of

the lattice, highlighted by the frequency dependency of the phase velocity, and the anisotropy of the domain in the wave propagation plane.

3. Wave propagation characteristics of hexagonal lattices

The techniques presented in the previous section are used to investigate waves propagating in the hexagonal lattices under investigation. Dispersion relations and wave velocities are computed for different parameters of the lattice, with focus on the effects of variations of the internal angle θ.

3.1. Dispersion relations

The dispersion relations are presented in the form of iso-frequency contours. The contours corresponding to the first branch for hexagonal lattices with $\alpha = 1$, $\beta = 1/15$ and varying internal angles (specifically $\theta = 30^\circ, 10^\circ, 0, -10^\circ$) are shown in Fig. 5. The periodicity of the dispersion relations in the wavenumber space defined by the k_1, k_2 pair is highlighted by the boundaries of the first Brillouin zone superimposed to the plot. It is interesting to observe how the shape of the contours and of the area of the first Brillouin zone change significantly with the internal angle. This suggests differences in the wave propagation characteristics of the lattices, and ultimately in their mechanical properties. For instance, Fig. 6 presents the dispersion contours over a smaller range of the wave vector, which corresponds to the low frequency/long wavelength, i.e. quasi-static behavior of the lattice. Representation in terms of the components of the wave vector in the physical space, denoted as ξ_1, ξ_2, allows a more immediate interpretation of the results. The circular contours for the

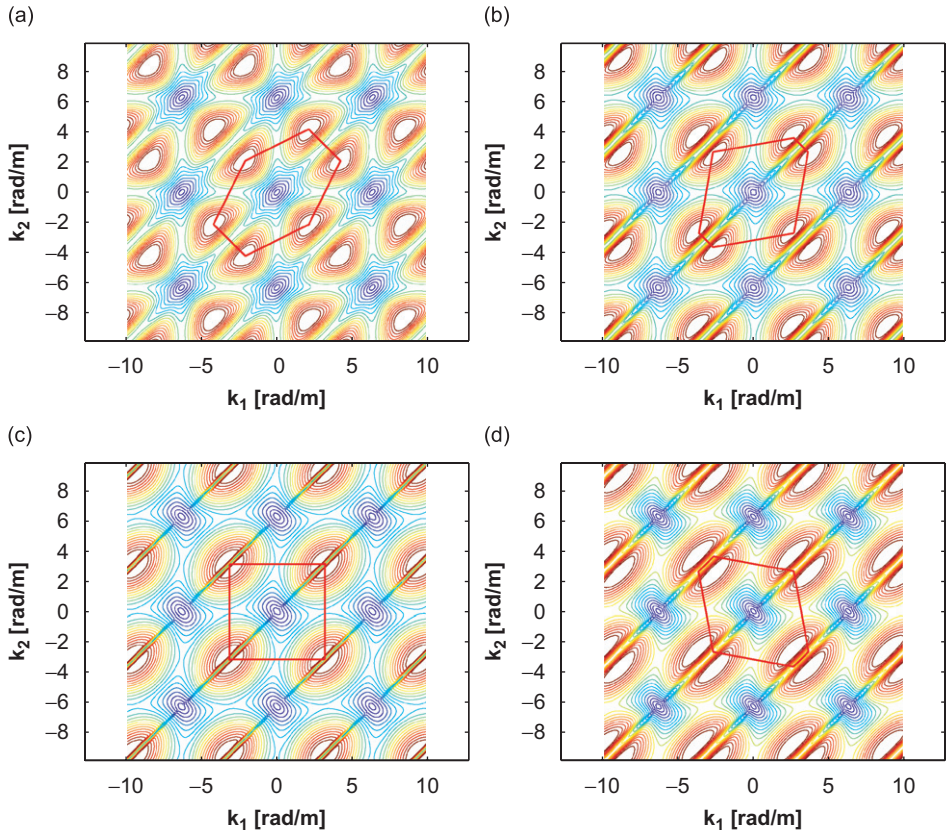

Fig. 5. Contour plots of dispersion relations (1st mode) for various lattice configurations: (a) $\theta = 30^\circ$, (b) $\theta = 10^\circ$, (c) $\theta = 0^\circ$, and (d) $\theta = -10^\circ$.

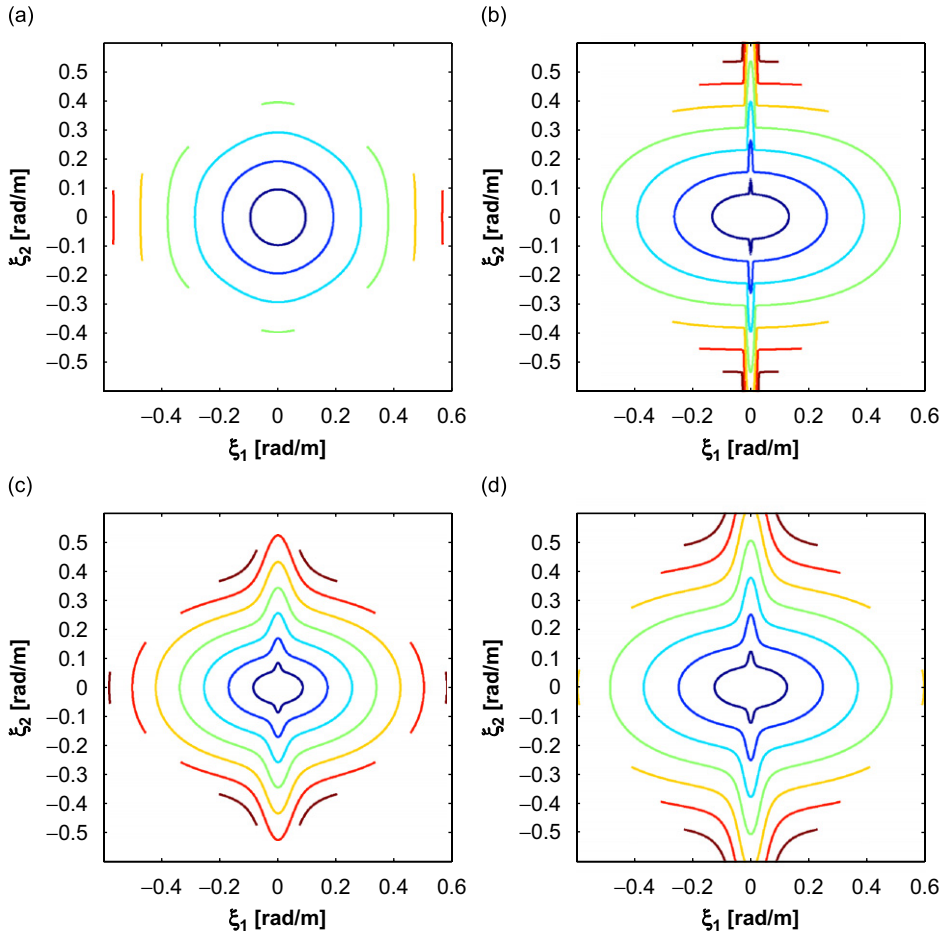

Fig. 6. Detail of low-frequency behavior of dispersion relations (1st mode) for various lattice configurations: (a) $\theta = 30^\circ$, (b) $\theta = 10^\circ$, (c) $\theta = 0^\circ$, and (d) $\theta = -10^\circ$.

regular hexagonal lattice ($\theta = 30^\circ$) suggest its isotropic behavior within the corresponding frequency range. The isofrequency contours can be considered as alternatives to slowness curves at a specified value of frequency, and as such, they can be used as a convenient representation of the isotropy, or lack of thereof, of a given elastic medium [12] along the plane of wave propagation. In contrast to the $\theta = 30^\circ$ case, the non-regular hexagonal geometries feature lobed isofrequency contours which indicate anisotropy even at low frequencies. Negative internal angles seem to produce a more accentuated lobe if compared with same values of positive internal angle. In addition, the lobe becomes very narrow for $\theta = 0^\circ$.

3.2. *Band structure*

A convenient and compact representation of the dispersion relations is obtained by varying the wave vector along the contour of the first Brillouin zone. For practical purposes, the symmetry of the first zone can be exploited to limit the variation of the wave vector along the irreducible zone, which can be defined as the smallest area allowing full representation of the $\omega = \omega(k_1, k_2)$ variation. The resulting representation shows the mode structure of the domain, and the presence of interesting wave phenomena such as for example mode veering and bandgaps [13,7]. The results shown in Fig. 5 show that the shape of the first Brillouin zone changes with the value of the internal angle. In particular, there is significant difference between lattices with positive and negative internal angles, with the case for $\theta = 0$ showing a peculiar quadrilateral shape, as opposed to the

hexagonal areas characterizing all other lattices. The irreducible zone and associated contour also change with θ, and it is in general larger than the one that can be selected in lattices with regular hexagonal geometry [7]. The first Brillouin zone for lattices with positive and negative internal angles are shown in Fig. 7, where the contours of the irreducible zones considered for the subsequent analysis are also highlighted as shaded areas. The Brillouin zones are here represented in the physical wavenumber space ξ_1, ξ_2.

Examples of band structure for several lattice configurations are shown in Figs. 8 and 9, where the frequency axis $\Omega = \omega/\omega_0$ is normalized with respect to the flexural resonance ω_0 of a simply supported

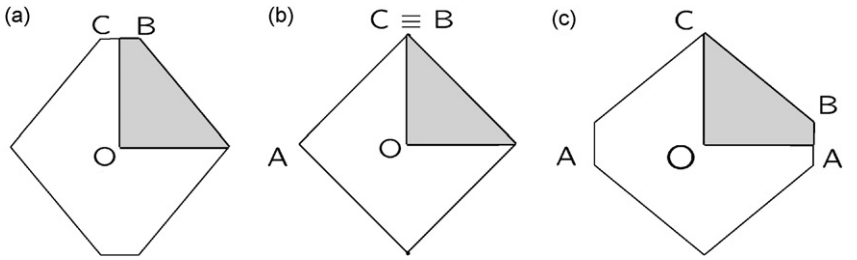

Fig. 7. Variation of First Brillouin Zone with internal angle: (a) $\theta > 0$, (b) $\theta = 0$, and (c) $\theta < 0$.

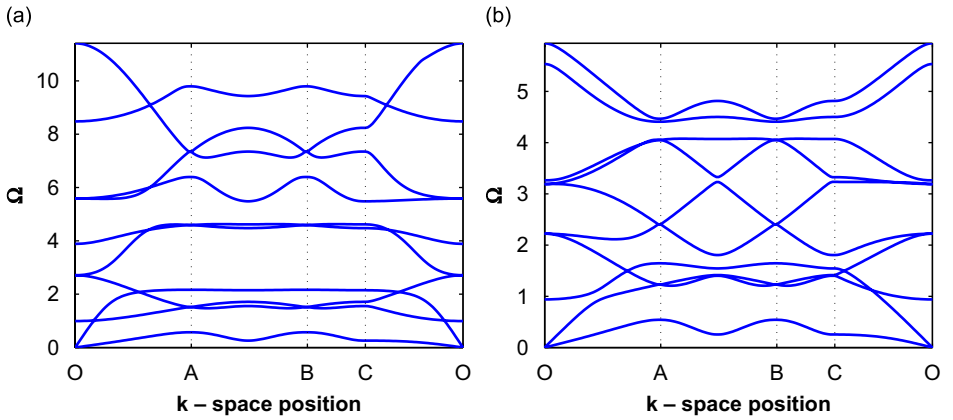

Fig. 8. Band structure for lattices with $\theta = 30^\circ$ and $\alpha = 1$: (a) $\beta = 1/15$ and (b) $\beta = 1/5$.

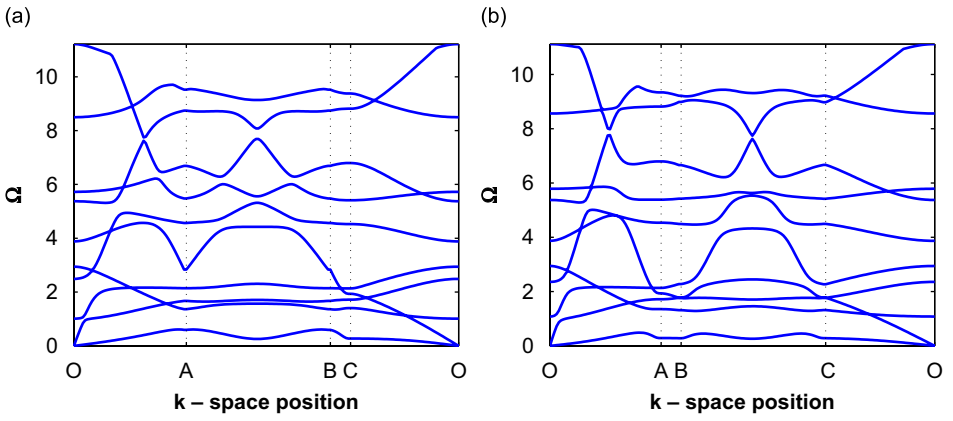

Fig. 9. Band structure for lattices with $\beta = 1/15$ and $\alpha = 1$: (a) $\theta = 10^\circ$, and (b) $\theta = -10^\circ$.

lattice beam of length L:

$$\omega_0 = \frac{\pi^2}{L^2}\sqrt{\frac{EI}{\rho t}} = \beta\pi^2\sqrt{\frac{E}{12\rho}}, \tag{22}$$

with ω denoting the frequency corresponding to the assigned wavenumber, E, ρ, I the material and inertia properties of the lattice beams and t the considered wall thickness defined in Fig. 2. Fig. 8 shows how the dispersion characteristics of a regular hexagonal lattice are influenced by the slenderness ration $\beta = t/L$. In the considered frequency range, the lattice with $\beta = 1/15$ features a bandgap for $\Omega > 5$, as well as veering of the branches at several locations. Veering consists in two branches coming infinitely close without crossing or touching, and it is a common phenomenon found in the solution of eigenvalue problems containing weakly coupled systems [13,14]. Changing the slenderness ratio β of the lattices causes a general increase in the modal density in the considered range of frequencies, and a significant alteration of the band structure. The increase in modal density is essentially due to the selected non-dimensional frequency expressed in Eq. (22), which is proportional to $\beta = t/L$. For a given set of parameters, increasing β corresponds to increasing ω_0 and therefore causing the non-dimensional parameter Ω to cover a broader frequency range. Remarkable is also the fact that, in the non-dimensional plots, the lower branch remains virtually unaffected by the change in

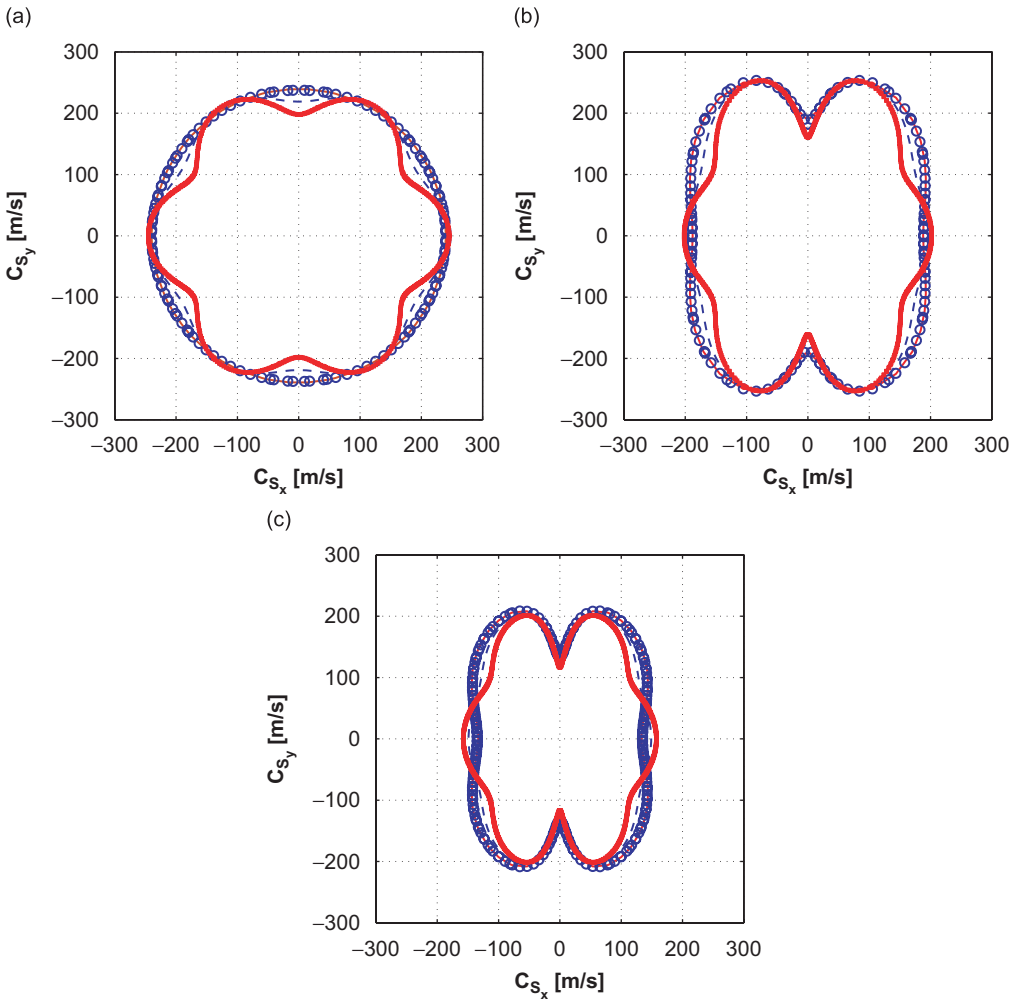

Fig. 10. S-mode: phase velocity variation for various lattices: (a) $\theta = 30°$, (b) $\theta = 10°$, (c) $\theta = -10°$ and at various frequencies: '-' $\Omega = 0.025$, 'o' $\Omega = 0.05$, '–' $\Omega = 0.15$, '*' $\Omega = 0.2$.

slenderness ratio. This branch corresponds to the shear mode of a homogeneous medium [7], and its slope defining the corresponding speed can be expressed in terms of equivalent shear modulus and density for the medium. In the case of hexagonal lattices, the equivalent shear modulus scales with the cube of the slenderness ratio, while the relative density scales with the slenderness ratio, i.e.:

$$G_{\mathrm{eq}} \propto \beta^3, \quad \rho_{\mathrm{eq}} \propto \beta. \tag{23}$$

Accordingly, at low frequencies, the first branch of the dispersion relation can be approximated as

$$\omega = k\sqrt{G_{\mathrm{eq}}/\rho_{\mathrm{eq}}} \propto \beta \tag{24}$$

and the non-dimensional quantity obtained by normalizing by ω_0 becomes independent from β. This confirms the predictions of the equivalent mechanical properties and their variations in terms of the slenderness ratio for hexagonal lattices.

The veering found between the $O \to A$ segment of the diagram for $\beta = 1/15$ disappears with the higher value of β as the two branches clearly separate. Similar observations can be made from the comparison of the band structure of lattices with $\theta = 10^\circ$ and -10° shown in Fig. 9. In both cases, there is a noticeable

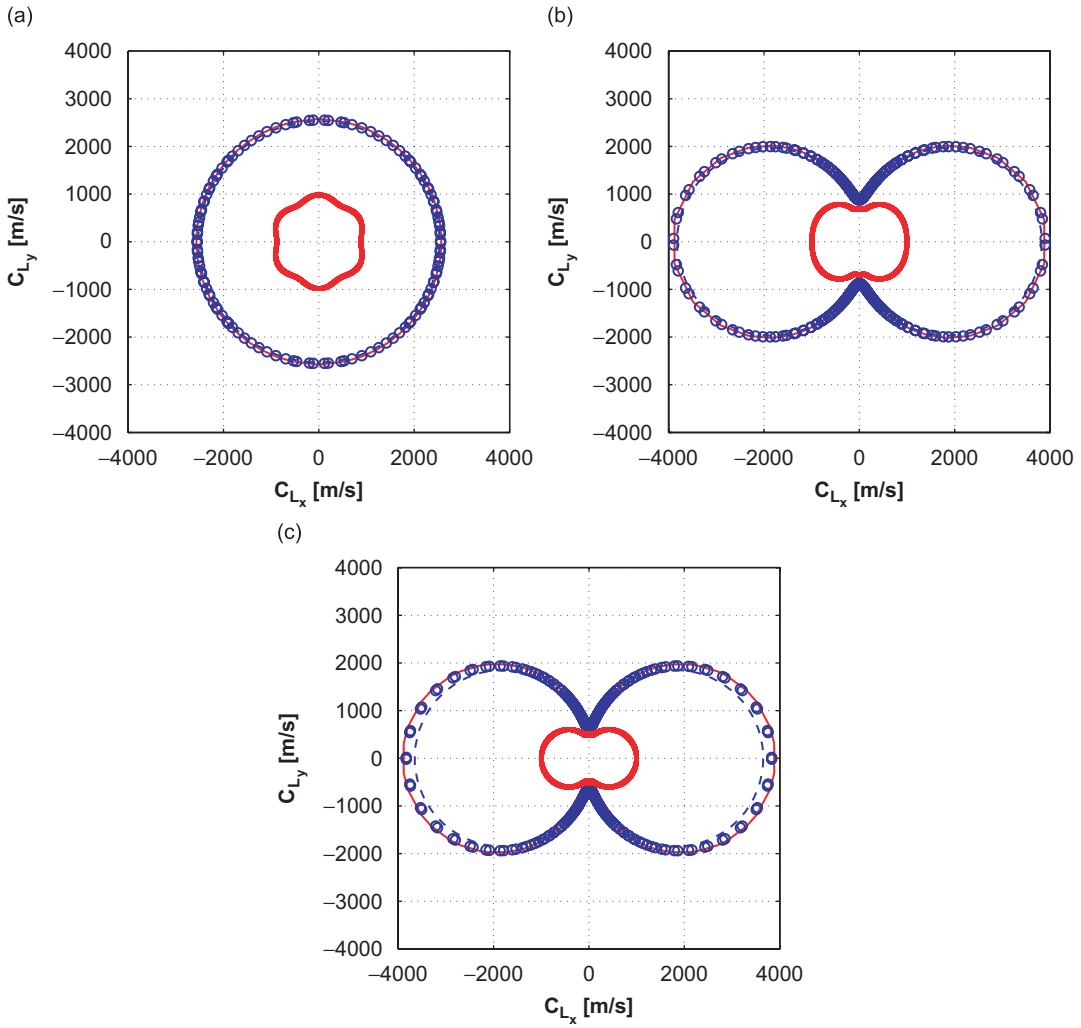

Fig. 11. L-mode: phase velocity variation for various lattices: (a) $\theta = 30^\circ$, (b) $\theta = 10^\circ$, (c) $\theta = -10^\circ$ and at various frequencies: '-' $\Omega = 0.025$, 'o' $\Omega = 0.05$, '–' $\Omega = 0.15$, '*' $\Omega = 0.2$.

absence of bandgaps and a general asymmetry of the diagrams which sets them apart from the ones of regular hexagonal lattices.

3.3. Phase and group velocities

Phase and group velocities are evaluated to highlight the non-isotropic behavior of the lattices, as well as their dispersive characteristics. In what follows, results are presented for velocities corresponding to the first branch of the dispersion diagram. For convenience, and in analogy with the behavior of a homogeneous solid, the corresponding mode is here denoted as "shear" (S-mode), while the one corresponding to the second branch is called "longitudinal" (L-mode).

The angular variation of the S-mode is shown in Fig. 10, which compares phase velocities for $\theta = 30^\circ$, 10°, -10° and $\alpha = 1$, $\beta = 1/15$ for increasing values of frequency. The regular hexagonal honeycomb behaves as an isotropic solid at low frequencies, as indicated by the corresponding circular velocity curve (Fig. 10a). It is interesting to observe also that the low-frequency behavior of the lattice appears as non-dispersive as the velocity curves at different frequencies overlap almost exactly. The non-isotropic behavior of the lattice appears evident from the curve at $\Omega = 0.2$ which features the six-fold, hexagonal symmetry of the lattice. The anisotropic behavior of the non-regular hexagonal lattices can be clearly observed from the variation of the

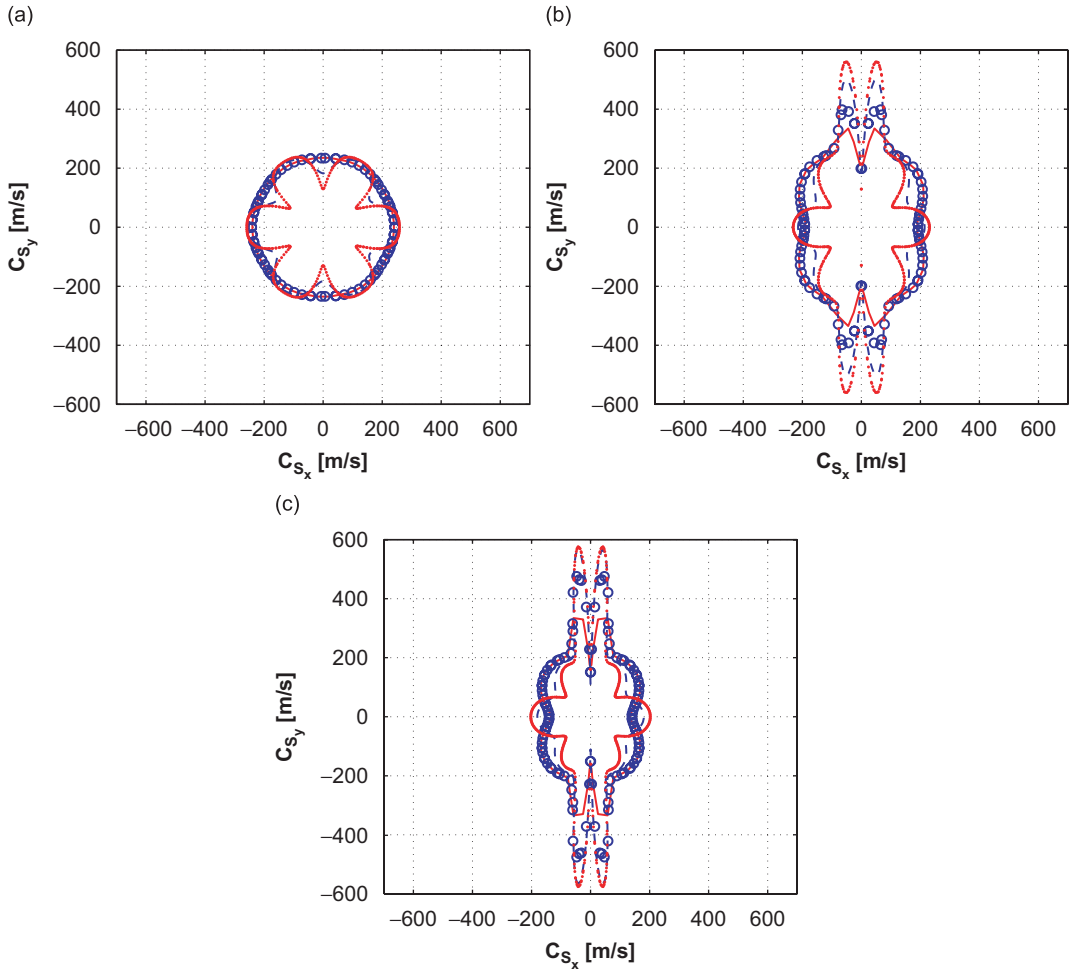

Fig. 12. S-mode: group velocity variation for various lattices: (a) $\theta = 30^\circ$, (b) $\theta = 10^\circ$, (c) $\theta = -10^\circ$ and at various frequencies: '-' $\Omega = 0.025$, 'o' $\Omega = 0.05$, '–' $\Omega = 0.15$, '*' $\Omega = 0.2$.

phase velocity shown in Fig. 10b,c, which also highlight the presence of a frequency range where the phase velocity is not dependent on frequency.

Similar considerations can be made from the analysis of the phase velocity curves for the L-mode (Fig. 11), which appear as non-dispersive over a broader frequency range, as demonstrated by the linear variation of the corresponding branch shown in the band structure diagrams. The anisotropic characteristics of the non-regular hexagonal lattices is also markedly visible, with a clear difference between velocities along horizontal and vertical directions.

Examples of variations of the group velocity for the first two modes are presented in Figs. 12 and 13. The results confirm the non-dispersive behavior at low frequencies for the regular lattice, as indicated by the frequency independent velocities in this frequency range, and by the match between group and phase velocities at a given frequency. The group velocities for the non-regular lattices show a remarkable difference due to the presence of high-velocity lobes appearing around the vertical direction and at higher frequencies. Such lobes directly correspond to the lobed nature of the dispersion relations presented in Section 3.1. The lobes appear more evident for the S-mode, whereas the longitudinal mode is characterized by a more regular angular

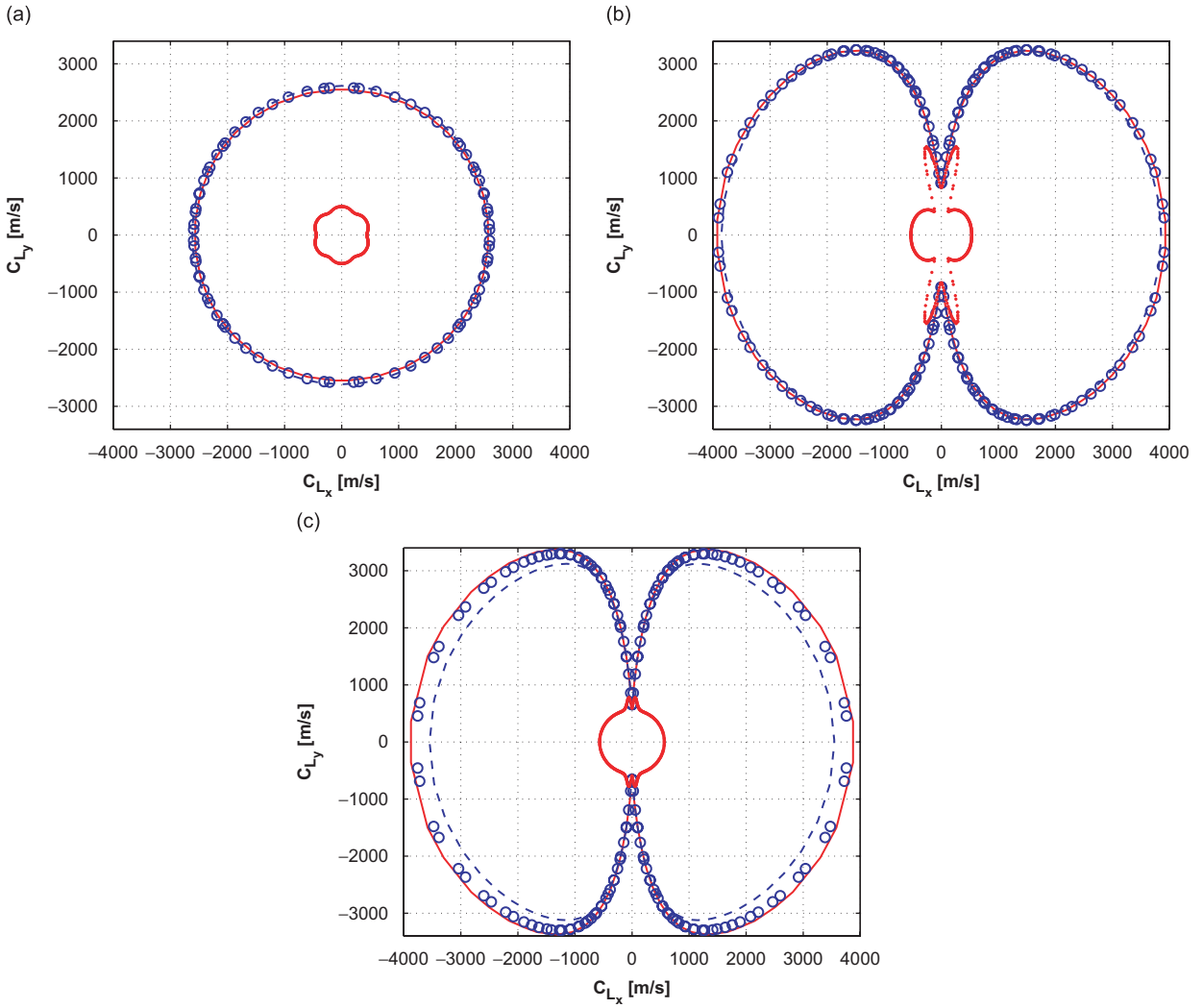

Fig. 13. L-mode: group velocity variation for various lattices: (a) $\theta = 30^\circ$, (b) $\theta = 10^\circ$, (c) $\theta = -10^\circ$ and at various frequencies: '-' $\Omega = 0.3$, 'o' $\Omega = 0.5$, '–' $\Omega = 0.7$, '*' $\Omega = 1.5$.

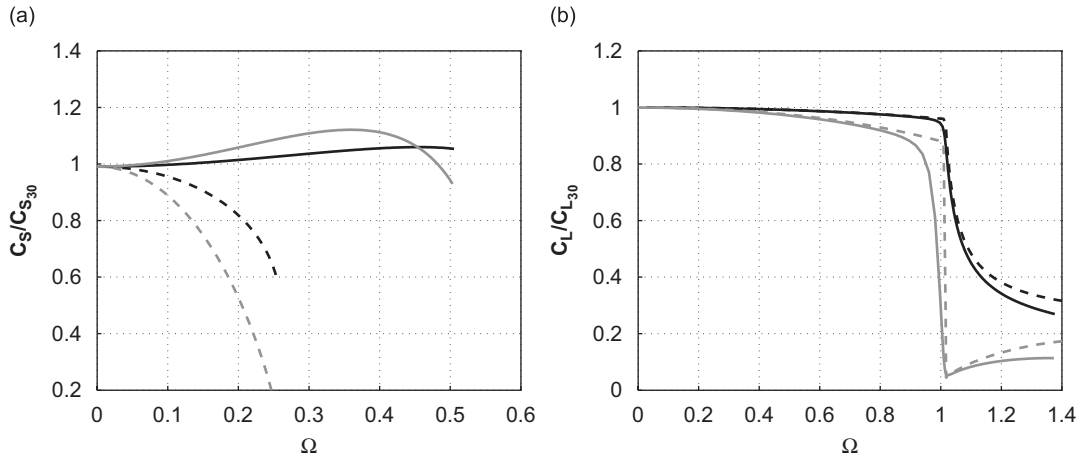

Fig. 14. Comparison between phase and group velocity for $\theta = 30^\circ$: (a) S-mode and (b) L-mode. C_{phase_x} solid black, C_{phase_y} dashed black, C_{group_x} solid gray, C_{group_y} dashed gray.

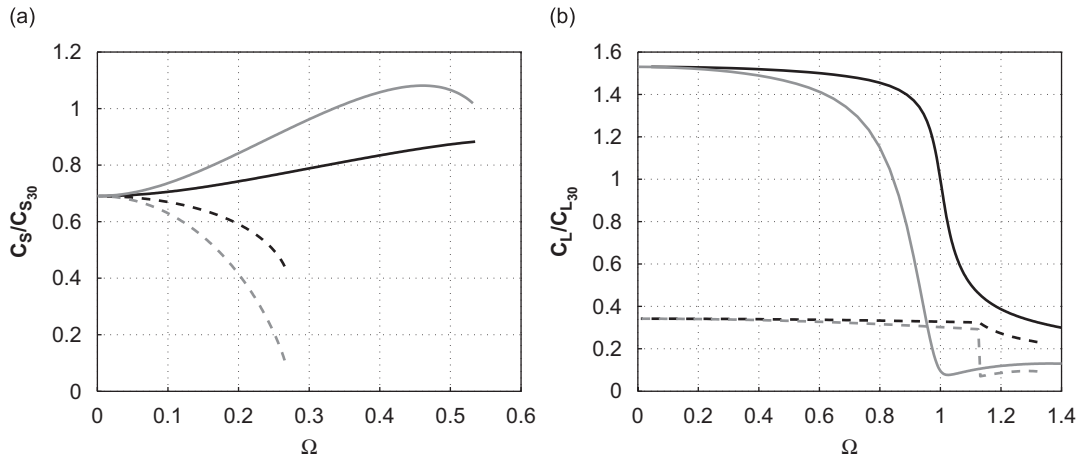

Fig. 15. Comparison between phase and group velocity for $\theta = 10^\circ$: (a) S-mode and (b) L-mode. C_{phase_x} solid black, C_{phase_y} dashed black, C_{group_x} solid gray, C_{group_y} dashed gray.

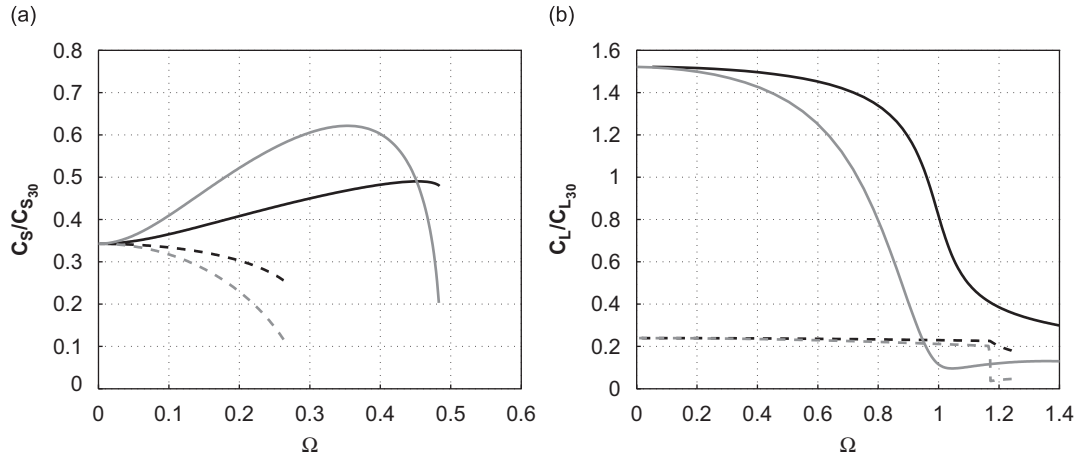

Fig. 16. Comparison between phase and group velocity for $\theta = -10^\circ$: (a) S-mode and (b) L-mode. C_{phase_x} solid black, C_{phase_y} dashed black, C_{group_x} solid gray, C_{group_y} dashed gray.

behavior. The plots of Figs. 12 and 13 clearly demonstrate the anisotropic behavior of the considered lattices, and show the influence of frequency on their wave propagation characteristics.

Direct comparison of phase and group velocities along the x, y directions for different lattices are shown in Figs. 14–16 where the vertical axes are normalized in terms of the corresponding velocities of the hexagonal lattice, here denoted as $C_{S_{30}}$ and $C_{L_{30}}$. It is finally interesting to note how the longitudinal mode behaves non-dispersively over a broader frequency range for all lattices.

4. Conclusions

The characteristics of wave propagation in hexagonal lattices was investigated. The considered approach consists of the application of unit cell analysis and the Bloch theorem to obtain dispersion surfaces and to allow the subsequent estimation of band structure, and wave velocities in terms of frequency and direction of wave propagation. The analysis of hexagonal lattices of varying internal angles highlights remarkable differences in the wave propagation characteristics, in particular as re-entrant configurations are considered. Such differences are evaluated through the investigation of the presence of bandgaps and veering, and the analysis of wave beaming and dispersion characteristics of the various lattice configurations.

Acknowledgments

The authors wish to thank Mr. Alessandro Spadoni from the School of Aerospace Engineering at Georgia Tech for the constant assistance and the many useful discussions during the early stages of this work.

References

[1] L. Brillouin, *Wave Propagation in Periodic Structures*, Dover, New York, 1953.
[2] D.J. Mead, A general theory of harmonic wave propagation in linear periodic systems with multiple coupling, *Journal of Sound and Vibration* 27 (1973) 235–260.
[3] R.S. Langley, The response of two dimensional periodic structures to point harmonic forcing, *Journal of Sound and Vibration* 197 (4) (1996) 447–469.
[4] O. Sigmund, J. Jensen, Systematic design of phononic band-gap materials and structures by topology optimization, *Philosophical Transactions of the Royal Society London, Series A (Mathematical, Physical and Engineering Sciences)* 361 (1806) (2003) 1001–1019.
[5] M. Ruzzene, F. Scarpa, F. Soranna, Wave beaming effects in two-dimensional cellular structures, *Smart Materials and Structures* 12 (3) (2003) 363–372.
[6] S.M. Jeong, M. Ruzzene, Analysis of vibration and wave propagation in cylindrical grid-like structures, *Shock and Vibration* 11 (3–4) (2004) 311–331.
[7] A.S. Phani, J. Woodhouse, N.A. Fleck, Wave propagation in two-dimensional periodic lattices, *Journal of the Acoustical Society of America* 119 (4) (2006) 1995–2005.
[8] A.R. Diaz, A.G. Haddow, L. Ma, Design of band-gap grid structures, *Structural Multidisciplinary Optimization* 29 (6) (2005) 418–431.
[9] L. Gibson, F. Ashby, *Cellular Solids. Structures and Properties*, Cambridge University Press, Cambridge, UK, 2001.
[10] P.G. Martinsson, A.B. Movchan, Vibrations of lattice structures and phononic bandgaps, *The Quarterly Journal of Mechanics and Applied Mathematics* 56 (2003) 45–64.
[11] E.A. Friis, R.S. Lakes, J.B. Park, Negative Poisson's ratio polymeric and metallic materials, *Journal of Materials Science* 23 (1988) 4406–4414.
[12] B.A. Auld, *Acoustic Fields and Waves in Solids*, second ed., Krieger Publ. Co., Malabar FL, 1990.
[13] N.C. Perkins, C.D. Mote, Comment on curve veering in eigenvalue problems, *Journal of Sound and Vibration* 106 (1986) 451–463.
[14] P.S. Nair, S. Duvarsula, On quasi-degeneracies in plate vibration problems, *International Journal of Mechanical Science* 15 (3–4) (1973) 975–986.